Heliyon 10 (2024) e35012

Contents lists available at ScienceDirect

Heliyon

journal homepage: www.cell.com/heliyon

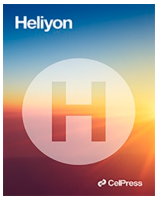

Research article

Upregulation of the tumor suppressor gene *LIN9* enhances tumorigenesis and predicts poor prognosis of lung adenocarcinoma

Qinghua Hou [a], Yanfeng Zhong [b], Mengying Liao [c], Chao Chen [a], Yanling Li [b], Xiaoqing Li [a], Jixian Liu [a,*]

[a] *Department of Thoracic Surgery, Peking University Shenzhen Hospital, Shenzhen, Guangdong, 518036, China*
[b] *Department of Central Laboratory, Peking University Shenzhen Hospital, Shenzhen, Guangdong, 518036, China*
[c] *Department of Pathology, Peking University Shenzhen Hospital, Shenzhen, Guangdong, 518036, China*

ARTICLE INFO

Keywords:
LIN9
Lung adenocarcinoma
Tumor suppressor gene
Cancer cell progression
Prognosis

ABSTRACT

Background: *LIN9*, a gene associated with various cancers, is considered a tumor suppressor. However, the role of *LIN9* in lung adenocarcinoma (LUAD) remains unknown. In this study, we aimed to assess the role of *LIN9* in the occurrence and prognosis of LUAD.
Methods: Using three-tier HTSeq count RNA sequencing data from The Cancer Genome Atlas, we assessed LIN9 expression for the LUAD dataset using the DESeq2 R package and RT-qPCR experiments. Biological functions were assessed using gene set enrichment analysis (clusterProfiler and GOplot). The expression of *LIN9* and the infiltration of immune cells were assessed by Single-sample gene set enrichment analysis. We conducted correlation study using clinical characteristics and receiver operating characteristic curve analysis. The predictive value of *LIN9* was determined using univariate and multivariate Cox regression as well as Kaplan-Meier analysis. Additionally, functional studies were conducted to validate its role in the progression of LUAD.
Results: Expression of *LIN9* was significantly elevated in LUAD, primarily influencing cell cycle, division, and signaling pathways. High *LIN9* expression correlated positively with the infiltration of Th2 cells and inversely with that of plasmacytoid dendritic cells. Furthermore, *LIN9* was associated with older age and advanced clinical stages, posing risks to overall, progression-free, and disease-specific survival. *LIN9* served as a good diagnostic marker, particularly in females, patients aged over 65, and those with clinical N1–3 and M1 stages. Elevated *LIN9* expression enhanced proliferation, migration, and invasion of LUAD cells.
Conclusion: High *LIN9* expression potentially contributes to LUAD occurrence through cell cycle regulation and chromosomal modification. It promotes the malignant characteristics of LUAD cells and holds prognostic value for affected patients.

1. Introduction

Based on the most recent data provided in 2020, lung cancer was the second most frequent and deadliest cancer globally, with a diagnosis rate of 11.4 % [1]. Lung cancer is traditionally categorized into two main types based on cellular origin: non-small cell lung

* Corresponding author.
E-mail address: liujx0417@163.com (J. Liu).

https://doi.org/10.1016/j.heliyon.2024.e35012
Received 17 December 2023; Received in revised form 14 July 2024; Accepted 22 July 2024
Available online 24 July 2024

cancer (NSCLC) and small cell lung cancer. Among these, NSCLC accounts for the majority of lung cancer cases and is further subdivided into several histological subtypes. Lung adenocarcinoma (LUAD) is recognized as the most prevalent subtype within the NSCLC category. LUAD represents a significant proportion of lung cancer diagnoses and is characterized by distinct pathological and molecular features [2]. Numerous gene targets developed for LUAD, including *EGFR*, *ALK*, *ROS1*, *BRAF*, and *RET*, have shown promising clinical results [3,4]. However, due to the limited number of clinically available molecular targets, the number of patients who benefit from such targets remains limited [5,6]. *LIN9* is a component of the conserved dimerization partner and multi-vulval class B (DREAM) complex, which was first discovered in Drosophila. It has been found to act as a suppressor of cell cycle regulating genes [7,8]. *LIN9* is a critical factor in the regulation of mitosis and has a significant part in the transcriptional regulation of G2/M cell cycle-associated gene expression. Previous studies have suggested that *LIN9* is associated with multiple types of cancer. cancers. *LIN9* functions as a suppressor of tumor growth [9]. Furthermore, some studies have indicated that *LIN9* associates and cooperates with pRB and that it has tumor suppressing activities [10]. However, the roles of *LIN9* in LUAD prognosis and progression remain unclear. Therefore, we conducted a novel investigation to examine the correlation between *LIN9* expression and the prognosis of LUAD, aiming to ascertain its prognostic significance and confirm its involvement in the development and occurrence of LUAD.

2. Materials and methods

2.1. Data processing and ethical statements

We obtained and compiled RNA-seq data that had been processed using the STAR approach from 33 cancer projects in the Tumor Genome Atlas Database (The Cancer Genome Atlas, TCGA, https://portal.gdc.cancer.gov/) and extracted the data in transcripts per million reads (TPM) format. This included sequence data for LUAD and corresponding clinical pathological data, totaling 516 and 59 tumor and normal samples, respectively (duplicates were removed, and samples with clinical information were retained). We extracted paired para-cancer and cancer samples by corresponding numbers and converted the TPM format of RNA-seq data to Log2(value + 1) values to compare expression between samples. Statistical analyses were performed using the stats and car packages within the R software environment. These analyses were carried out only if the data satisfied the necessary statistical prerequisites. In instances where the data did not meet these requirements, statistical analysis was not conducted. To effectively visualize the data, we utilized the ggplot2 package, which is well-regarded for its robust and flexible plotting capabilities. The dataset employed in this study was obtained from TCGA, which adheres to stringent guidelines to ensure data accessibility and integrity. According to these guidelines, all participants involved in the study provided written informed consent prior to the collection and use of their data.

2.2. Identification and functional enrichment of differentially expressed LUAD genes

LUAD samples containing clinical information were retained, and duplicates were removed. Using the median expression of *LIN9* as a criterion, the 516 patients with LUAD were categorized into two groups: *LIN9* high-expression and *LIN9* low-expression. The DESeq2 R program [11] was utilized to detect differentially expressed genes (DEGs) among the groups. The threshold was defined as a $|\log$ fold change (logFC)$|\geq$ 1.5 and an adjusted P-value $\leq$0.05. Afterwards, the Spearman approach was used to assess genes that showed positive and negative correlation with *LIN9* expression. The R program ggplot2 was utilized to visually represent the DEGs and their linked genes through volcano plots and heatmaps, respectively. The differentially expressed genes (DEGs) were subjected to enrichment analysis for Gene Ontology (GO) terms and Kyoto Encyclopedia of Genes and Genomes (KEGG) pathways. This analysis was performed using the R packages clusterProfiler and GOplot. The LogFC values were taken into consideration to ensure accurate identification and interpretation of enriched biological processes and pathways. The DEG inputs were transformed into Entrez IDs using the org.Hs.eg.db package. The clusterProfiler software was utilized to do enrichment analysis. Using the LogFC value of DEGs, the z-score value of each enrichment entry was calculated via the GOplot package, initially determining whether the corresponding entries were positively (positive z-score) or negatively regulated (negative z-score), $zscore = \frac{(UP-DOWN)}{\sqrt{counts}}$ ("Up" and "Down" represent the number of entries for which the logFC of the corresponding items is positive or negative, respectively. "Counts" represents the total number of corresponding items).

2.3. Protein–protein interaction network

The interaction network of the *LIN9* protein was analyzed using the STRING database, which can be accessed at http://string-db.org. For this study, a minimum interaction score of 0.7 was required to ensure high confidence in the results. For every pair of protein interactions, the database offers a detailed score that ranges from 0 to 1. A higher score denotes a more reliable protein-protein interaction(PPI).

2.4. Correlation analysis of LIN9 gene expression with immune cell infiltration and chemokines in LUAD

Initially, we utilized the single-sample Gene Set Enrichment Analysis (ssGSEA) method from the R package GSVA [12] to assess the immune infiltration characteristics within the LUAD dataset. This approach involved a detailed examination of 24 commonly studied immune cell types to identify their specific contributions and prevalence in the LUAD samples [13]. By applying ssGSEA, we were able to systematically quantify the abundance and activity of these immune cell types, thereby gaining insights into the immune landscape

associated with LUAD.Subsequently, we analyzed the relationship between *LIN9* expression levels and immune chemokines in LUAD using the TISIDB database (http://cis.hku.hk/TISIDB/), selecting chemokines based on Spearman correlation values of |rho| above 0.2 and a P-value below 0.01. The Spearman's rho value is a measure of rank correlation between two variables. In the event that the rho value is high, it indicates that the variables are positively linked. Conversely, if the rho value is negative, it indicates that the variables are negatively connected.

2.5. Clinical significance analysis of LIN9 expression in LUAD

To elucidate the clinical significance of *LIN9* expression, we selected the following clinical indicators: T, N, and M stages, gender, age, pathological stage, and post-treatment effects. Receiver operating characteristic (ROC) curve analysis was employed to assess the accuracy of *LIN9* expression levels in differentiating between LUAD and non-tumor tissues, with the aim of evaluating its predictive utility in diagnosing LUAD. The prognosis for patients with LUAD was analyzed using the Kaplan–Meier method. Subsequently, the proportion hazard assumption test was conducted using the survival package in R, and uni- and multivariate COX regression analyses were performed to study the possibility of *LIN9* being an independent risk factor for LUAD. We identified overall survival (OS), disease-specific survival (DSS), and progression-free interval (PFI) as the three prognostic indicators. The clinical variable selection strategy forwarded samples with a P-value below 0.1 in the univariate analysis to the multivariate COX analysis for model building. In multivariable Cox regression, the criterion for identifying risk factors was a P-value below 0.05.

2.6. Expression of LIN9 in LUAD cells and transfection of tumor cells

RNA was isolated from BEAS 2B (normal) and H1395 (LUAD) cell lines using the RNAfast200 kit (Shanghai Feijie). RNA concentration was measured with a NanoDrop 2000c (Thermo Fisher Scientific), ensuring an OD260/280 ratio between 1.8 and 2.1. Reverse transcription was conducted using the ReverTra Ace qPCR RT kit (Toyobo, FSQ-101) with 10 μg of RNA. Real-time PCR (RT-PCR) analysis was performed on the Roche LightCycler 480 system to assess *LIN9* gene expression, using primers: LIN9-F: TTTGATAGGACAGGGCTTGG, LIN9-R: TTTACTTCTCCACGGCGACT, GAPDH-F: ACAACAGCCTCAAGATCATCAGC, and GAPDH-R: GCCATCACGCCACAGTTTCC. The thermal cycling conditions consisted of an initial denaturation step at 95 °C for 5 min, followed by amplification cycles at 95 °C for 10 s and an annealing temperature of 60 °C for 30 s. SYBR Green Realtime PCR Master Mix (Toyobo, QPK-212) was used in the analysis. Subsequently, tumor cells were transfected separately with si-LIN9 and si-NC using LipofectamineTM2000 during the logarithmic growth phase, which resulted in two distinct groups: the si-LIN9 and the si-NC group. After transfection, the culture medium was changed out for a new double antibody media, and the cells were allowed to sit in a CO^2 incubator at 37 °C for four to 6 h. Samples were further cultured in the incubator for 48–72 h. The forward strand sequence of si-LIN9 was 5′- GCAUAAAGUUCAACAGUAUTT -3′, while its reverse complement sequence was 5′- AUACUGUUGAACUUUAUGCTT -3′. The forward strand sequence of si-NC was 5′- UUCUCCGAACGUGUCACGUTT-3′, while its reverse complement sequence was 5′- ACGUGACACGUUCGGAGAATT-3′. Silencing efficiency after transfection was assessed using RT-qPCR as described above.

2.7. Cell proliferation assay

Following the trypsinization procedure, the processed cells were accurately counted. Precisely 1000 cells were seeded into each well of a 96-well plate, with each well containing 100 μL of culture medium to ensure optimal growth conditions. The plate was then placed in a CO_2 incubator, which was maintained at a constant temperature of 37 °C to simulate physiological conditions. The cells were allowed to incubate for three different time intervals: 0 h, 48 h, and 72 h, to observe their growth and behavior over time.After the specified incubation periods, 10 μL of CCK-8 solution (Solarbio, Catalog No.: CA1210) were added to each well. This reagent is used to assess cell viability and proliferation. The plate was then incubated for an additional 1–2 h to allow the CCK-8 solution to interact with the cells. Following this incubation, a microplate reader was employed to measure the absorbance at 450 nm. This absorbance measurement is indicative of the number of viable cells in each well, providing data on cell proliferation over the course of the experiment.

2.8. Migration assay

A six-well plate was seeded with around 5×10^5 cells. After the cells adhered to the surface, a scratch was created in the layer of cells using a pipette tip that was aligned with a ruler. The cells were subsequently rinsed three times with phosphate buffered saline (PBS) to eliminate detached cells, and a new culture medium was introduced. The plate was placed in a 5 % CO_2 incubator and kept at a temperature of 37 °C. Photographs were taken using a microscope at 0 and 24 h. We used the following calculation to get the migration rate at 24 h:

$$\frac{(\textit{Width of scratch at } 0\ h\ -\ \textit{Width of scratch at } 24\ h)}{\textit{Width of scratch at } 0\ h}\ x\ 100\%.$$

2.9. Cell invasion assay

The Transwell chamber was inserted into a pre-chilled 24-well plate, and 100 μL of diluted Matrigel (diluted at a ratio of 1:8 with

serum-free Dulbecco's Modified Eagle Medium [DMEM]) was introduced into each well. Prior to incubation, the samples were chilled for a duration of 30 min, allowing the gel to solidify over a period of 4–5 h. The leftover liquid was extracted, and the samples were rehydrated with 100 μL of serum-free DMEM for an additional 20 min. Cell suspensions were created by mixing cells in serum-free DMEM, quantifying using a hemocytometer, and placing around 1×10^4 cells in the upper chamber. DMEM supplemented with 10 % fetal bovine serum was introduced into the lower chamber and incubated at 37 °C with CO^2. Following a 24-h period of culturing, the medium was removed, and the cells were rinsed once with PBS. Subsequently, the cells were treated with a 4 % formaldehyde solution for 15 min, stained with a crystal violet solution for 20 min, rinsed again with PBS, and seen under a microscope.

2.10. Statistic analysis

We used the R software (version 4.1.1) and GraphPad (primer6) for statistical analysis and visualization, and the Perl software (v5.30.0 Strawberry version for data organization. The immune infiltration and chemokine levels were analyzed using the Spearman correlation test. For the analysis of multiple groups, the Kruskal–Wallis test was utilized. The comparison of clinical and pathological characteristics between the high- and low-expression groups of *LIN9* was performed using either the Wilcoxon rank-sum test for continuous variables or the Pearson chi-square test. The p-value was calculated using the Log-Rank test alongside Kaplan-Meier survival analysis. All cell experiments were conducted in triplicate. Data analysis was carried out using t-tests, and the results were expressed as the mean ± standard deviation ($\overline{x} \pm SD$). P-value <0.05 was deemed statistically significant.

3. Results

3.1. Aberrant expression of LIN9 in different tumors and associated lesions of LUAD

Based on TCGA data, we performed a Wilcoxon rank-sum test to examine the expression of *LIN9* mRNA in different tumor types. Out of 33 tumor types analyzed, 17 malignancies had significantly higher levels of *LIN9* ($P < 0.05$), as illustrated in Fig. 1a. Moreover, our analysis of paired samples from the TCGA-LUAD dataset containing 58 LUAD samples revealed that *LIN9* was significantly more expressed in LUAD tissues than in adjacent normal tissues ($P < 0.001$, Fig. 1b). In addition, our RT-qPCR experiment verified that the expression level of *LIN9* was markedly elevated in H1395 LUAD cells compared to normal lung epithelial cells. ($P < 0.001$, Fig. 6a).

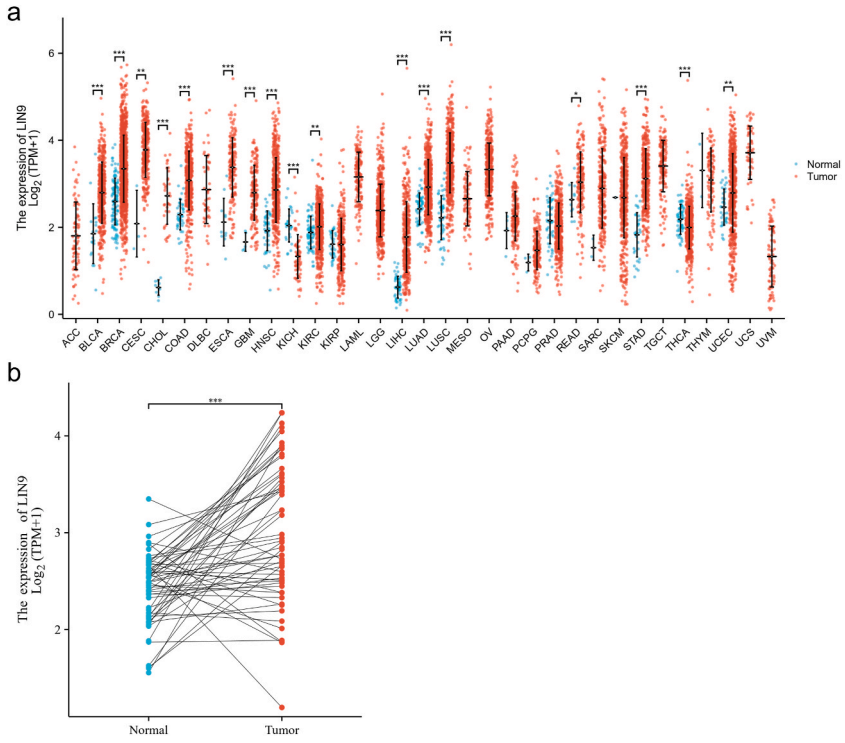

Fig. 1. Difference in expression of LIN9 between lung adenocarcinoma and pancarcinoma. (a) Expression of LIN9 in pancarcinoma. (b) Expression of LIN9 in paired lung adenocarcinoma samples.

3.2. Finding and annotating LIN9-associated DEGs functionally in LUAD

Next, we compared the DEGs between the *LIN9* high- and low-expression groups, resulting in a total of 518 DEGs being identified (Fig. 2a, Supplementary Table 1), including 268 protein coding RNAs (127 upregulated and 141 downregulated). Subsequently, we performed a correlation analysis for *LIN9* expression and used a heatmap to display the top five representative genes that exhibited the highest positive or negative correlations with *LIN9* expression (Fig. 2b). To elucidate the functional roles of LIN9-related DEGs in LUAD, enrichment analysis was conducted on 518 DEGs that were successfully converted into 358 Entrez IDs. The findings demonstrated the involvement of LIN9-related differential genes in a variety of biological processes, cellular elements, and molecular activities, such as cilium movement (GO:0003341), axoneme formation (GO:0005930), histone deacetylase binding (GO:0042826), and neuroactive ligand-receptor interaction (hsa04080; Fig. 2c–Table 1). The genes interacting with *LIN9* are shown in Fig. 2d.

3.3. Relationship of LIN9 expression to immune cell infiltration and chemokines

The ssGSEA algorithm was employed to assess the invasion of 24 immune cell types in LUAD (Fig. 3a). The Spearman's approach was utilized to examine the correlation between immune cell infiltration and LIN9 expression. (Fig. 3a). Notably, a positive correlation was observed between *LIN9* expression and Th2 cells ($R = 0.495$, $P < 0.001$), indicating a robust association. Conversely, pDCs exhibited a negative correlation with *LIN9* expression ($R = -0.347$, $P < 0.001$), further highlighting a strong association (where $|R|$ represents the magnitude of the correlation). Chemokine analysis in LUAD identified ten chemokines that were most tightly correlated with *LIN9*. Among these chemokines, only CCL26 showed a positive correlation with *LIN9* expression (rho = 0.201, $p < 0.01$). The chemokines CCL14, CCL17, CCL19, CCL22, CCL23, CX3CL1, CXCL14, CXCL16, and CXCL17 were negatively correlated with *LIN9*

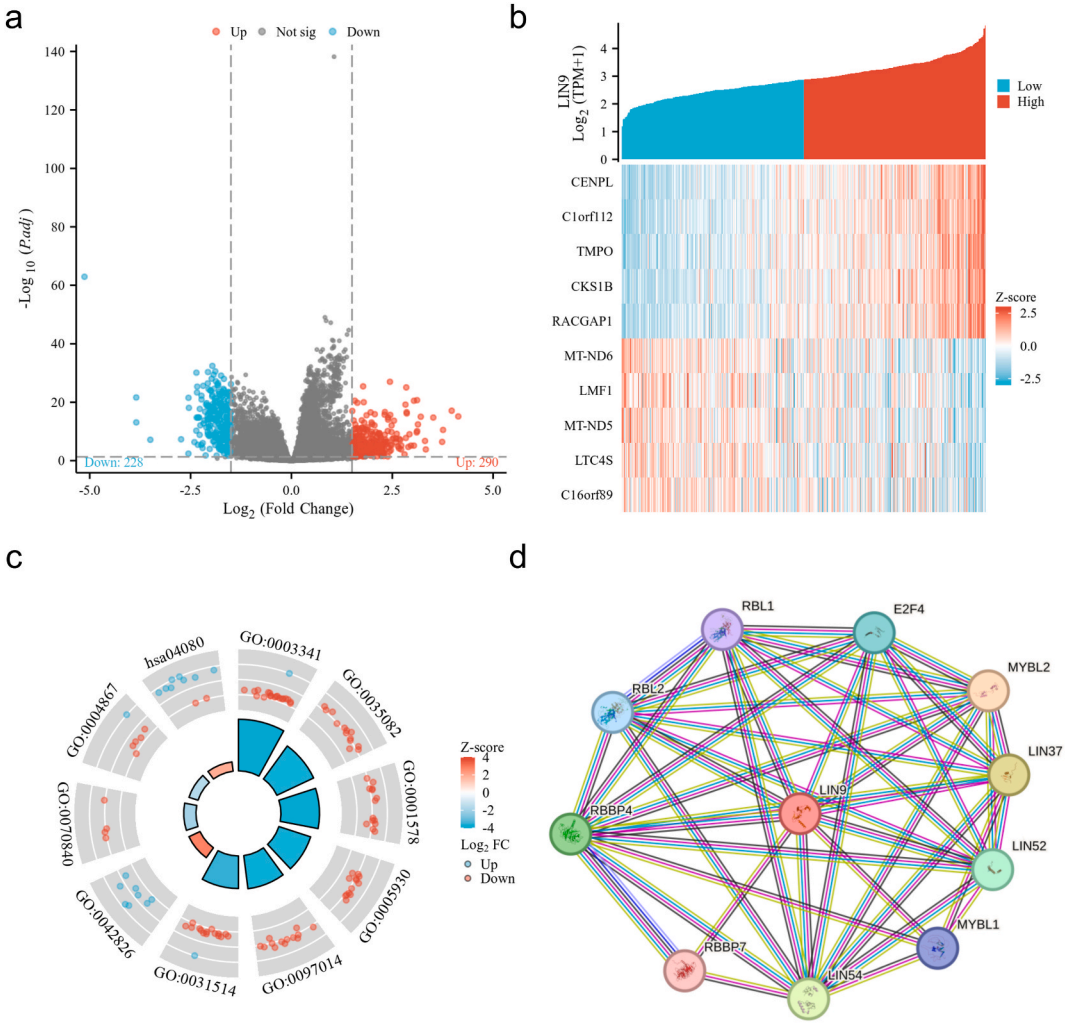

Fig. 2. LIN9-associated differential genes (DEGs) and functional annotation. (a) DEG volcano map. (b) Co-expression gene heat map. (c) GO/KEGG enrichment analysis. (d) PPI network.

Table 1
Functional enrichment analysis of GO/KEGG combined with logFC.

Ontology	ID	Description	p.adjust	zscore
BP	GO:0003341	cilium movement	8.08e-11	−4.0249
BP	GO:0035082	axoneme assembly	1.77e-08	−3.6056
BP	GO:0001578	microtubule bundle formation	4.79e-08	−3.7417
BP	GO:0007018	microtubule-based movement	4.69e-07	−4.264
BP	GO:0060294	cilium movement involved in cell motility	2.45e-06	−3.0509
CC	GO:0005930	axoneme	6.2e-07	−3.6056
CC	GO:0097014	ciliary plasm	6.2e-07	−3.6056
CC	GO:0031514	motile cilium	9.36e-07	−3.5
CC	GO:0097729	9 + 2 motile cilium	8.66e-05	−2.7136
CC	GO:0032838	plasma membrane bounded cell projection cytoplasm	9.74e-05	−3.6056
MF	GO:0042826	histone deacetylase binding	0.0222	2.8284
MF	GO:0070840	dynein complex binding	0.0222	−2
MF	GO:0004867	serine-type endopeptidase inhibitor activity	0.0855	−1.633
MF	GO:0004866	endopeptidase inhibitor activity	0.0855	−0.70711
MF	GO:0030414	peptidase inhibitor activity	0.0872	−0.70711
KEGG	hsa04080	Neuroactive ligand-receptor interaction	0.0947	1.8974

expression (Fig. 3b–k). These findings suggest that elevated *LIN9* expression influenced the infiltration patterns of distinct immune cell populations in LUAD tissues and the expression of various chemokines. It is important to note that the criteria we used to filter the TCGA LUAD data may have differed from the criteria used by the TISIDB database for chemokine analysis. This discrepancy in filtering criteria can lead to differences in the number of samples.

3.4. Association between LIN9 expression and clinical pathological characteristics in LUAD and its prognostic value

We compiled clinical information from 516 LUAD samples with variable handling of missing data across the samples, the baseline features of LUAD patients are listed in Table 2. The samples were categorized into two groups based on the median expression value of *LIN9*: high and low-expression groups. The statistical analyses demonstrated substantial disparities in several clinical variables between the two groups, such as T stage, M stage, gender, and main treatment result. (Table 2). An analysis of clinical characteristics within the group revealed a significant association between high *LIN9* expression and T stage (T1 vs. T2, $P < 0.001$), M stage (M0 vs. M1, $P < 0.001$), pathologic stage (stages I and II vs. stages III and IV, $P < 0.001$), gender (female vs. male, $P < 0.001$), and primary therapy outcome (PD vs. CR, $P < 0.01$; Fig. 4a–g). High levels of *LIN9* expression have been shown to function as an independent risk factor for OS, DSS, and PFI in uni- and multivariate Cox regression analysis. (Tables 3–5). The findings indicate that compared to LUAD with low *LIN9* expression, LUAD with high *LIN9* expression was more likely to progress to later stages and metastasize distantly. Notably, we observed a gender difference in *LIN9* expression in LUAD, with significantly higher levels in female patients than in male patients, and a higher disease control rate can be achieved. To investigate the value of *LIN9* in distinguishing LUAD from normal samples, we performed ROC curve analysis. As shown in Fig. 4h, ROC curve analysis revealed a ROC value for *LIN9* of 0.735 (95 % CI: 0.685–0.785). The results indicate that the high-LIN9 group had considerably reduced OS ($P < 0.001$), DSS ($P < 0.001$), and PFI ($P = 0.0100$) than the low-LIN9 group (Fig. 5a–c).

3.5. Enhanced expression of LIN9 promotes the progression of LUAD cells

Experiments on cellular function were performed to investigate the involvement of *LIN9* in LUAD progression. The CCK-8 analysis showed that the si-LIN9 group cells had a significantly lower ability to proliferate compared to the si-NC group. The OD values at 48 and 72 h were 0.50 ± 0.02 and 0.72 ± 0.03, respectively ($P < 0.01$; Fig. 6b). The scratch test results revealed a decreased migration rate of 7.00 ± 0.43 % in the si-LIN9 group at 24 h, which was statistically significant when compared to the si-NC group ($P < 0.05$; Fig. 6c). The Transwell experiment results indicated a significantly low number of H1395 cells passing through the basement membrane in the si-LIN9 group, with a relative invasion rate of 0.35 ± 0.03 ($P < 0.01$; Fig. 6d).

4. Discussion

LIN9 serves as a scaffold protein that constitutes the DREAM complex and plays three vital roles in oncogenic processes. First, it participates in and regulates the synthesis of multiple vulval class B (MuvB) and DREAM complexes. Overconsumption can directly reduce the synthesis of both, as well as induce downregulation of LIN37 and LIN54, which are other components within the MuvB complex, thereby further impacting synthesis. Additionally, *LIN9* expression is subject to feedback regulation via interactions between its upstream promoter and the DREAM complex [14]. Second, *LIN9* is a crucial regulator of mitosis and plays a significant role in the transcriptional regulation of G2/M cell cycle-related gene expression. *LIN9*, as a component of the MuvB complex, plays a critical role in cell cycle regulation by interacting with transcription factors BMYB and FOXM1. This interaction facilitates the activation of a suite of cell cycle genes specifically associated with the S, G2, and M phases. Through these molecular interactions, *LIN9* contributes to the precise temporal control of gene expression necessary for cell cycle progression and division, highlighting its importance in cellular

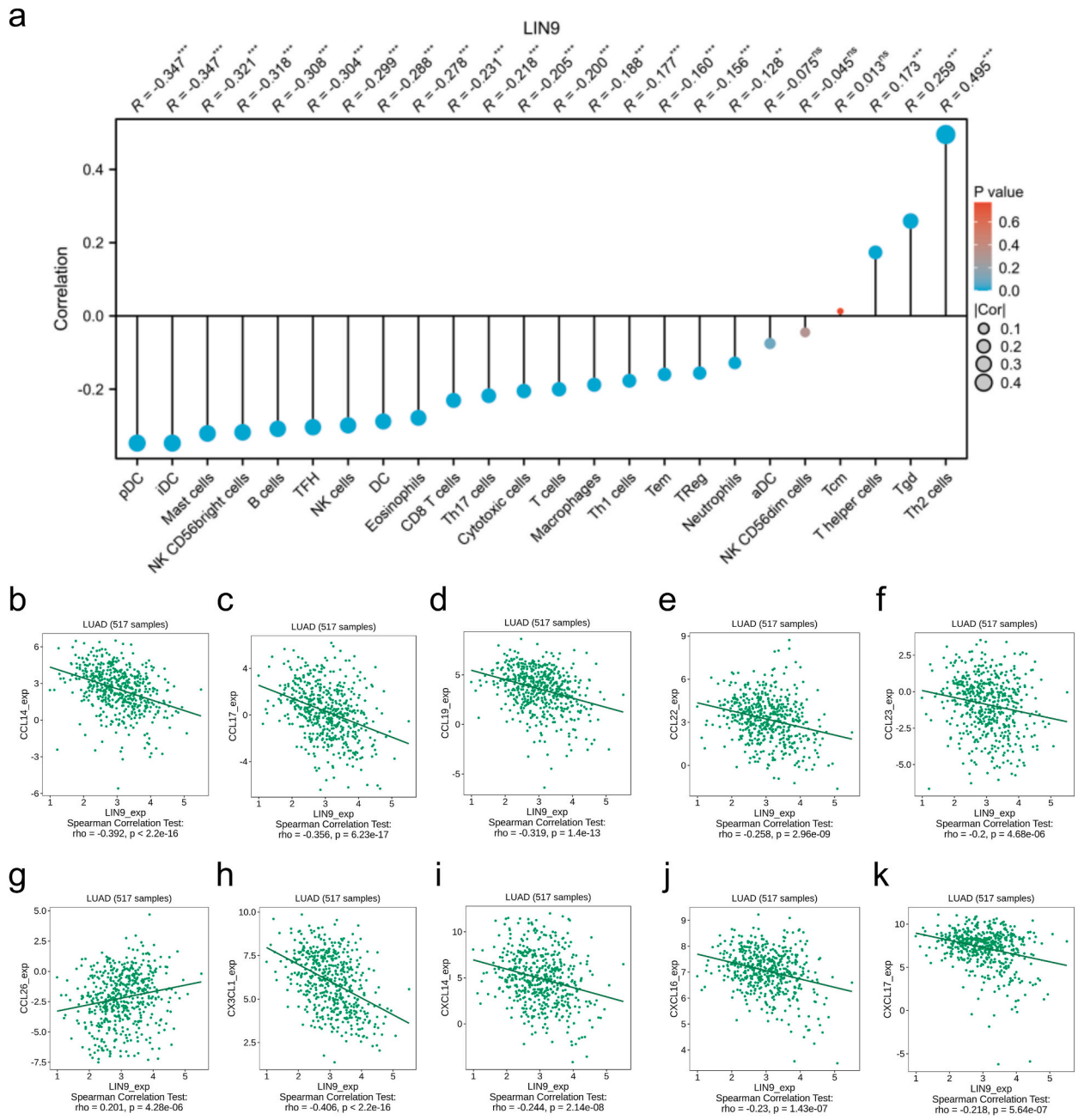

Fig. 3. Association of LIN9 with immune infiltration and chemokines. (a) Immune cell infiltration. (b–k) Chemokine expression.

proliferation and its potential as a target in cancer therapy [15–19]. Finally, as a tumor suppressor gene, it not only synergistically inhibits tumorigenesis and oncogenesis by binding to pRb but also activates the p53 signaling pathway to mediate cell apoptosis, inhibits rapid tumor cell proliferation, and prevents immune evasion [20]. Its tumor-suppressing function is not affected by pRb-mediated cell cycle inhibition or E2F-dependent reverse activation, and it can maintain its ability to activate transcription and promote differentiation when pRb mutates [10]. However, in our study, *LIN9* did not seem to function as a tumor suppressor gene but rather promoted the development of LUAD.

To our knowledge, there are currently no studies that have reported on the expression levels of *LIN9* and its potential impact on the prognosis of lung adenocarcinoma (LUAD). Consequently, our study aims to explore the potential role of *LIN9* in LUAD. We used high-throughput RNA sequencing data from the TCGA database to perform a bioinformatic study. This analysis revealed notable individual variability and heterogeneity in RNA transcripts across LUAD samples. Our findings indicate that *LIN9* is significantly upregulated in LUAD patients, suggesting that *LIN9* may serve as a potential diagnostic biomarker for this type of cancer.Our research identified that

Table 2
Clinicopathological features of LUAD with differential expression of *LIN9* (data on missing clinical variables are not presented in contingency Table 2).

Characteristics	Low expression of LIN9	High expression of LIN9	P value
n	258	258	
Pathologic T stage, n (%)			0.006
T1	102 (19.9 %)	67 (13.1 %)	
T2	126 (24.6 %)	152 (29.6 %)	
T3&T4	30 (5.8 %)	36 (7 %)	
Pathologic N stage, n (%)			0.907
N0	169 (33.5 %)	163 (32.3 %)	
N1	47 (9.3 %)	49 (9.7 %)	
N2&N3	37 (7.3 %)	39 (7.7 %)	
Pathologic M stage, n (%)			0.017
M0	169 (45.4 %)	178 (47.8 %)	
M1	6 (1.6 %)	19 (5.1 %)	
Pathologic stage, n (%)			0.242
Stage I&Stage II	206 (40.6 %)	192 (37.8 %)	
Stage III&Stage IV	50 (9.8 %)	60 (11.8 %)	
Age, n (%)			0.258
≤ 65	112 (22.5 %)	127 (25.6 %)	
> 65	134 (27 %)	124 (24.9 %)	
Gender, n (%)			0.003
Female	156 (30.2 %)	122 (23.6 %)	
Male	102 (19.8 %)	136 (26.4 %)	
Primary therapy outcome, n (%)			0.013
PD	24 (5.6 %)	44 (10.3 %)	
SD	19 (4.4 %)	18 (4.2 %)	
PR	3 (0.7 %)	3 (0.7 %)	
CR	181 (42.3 %)	136 (31.8 %)	

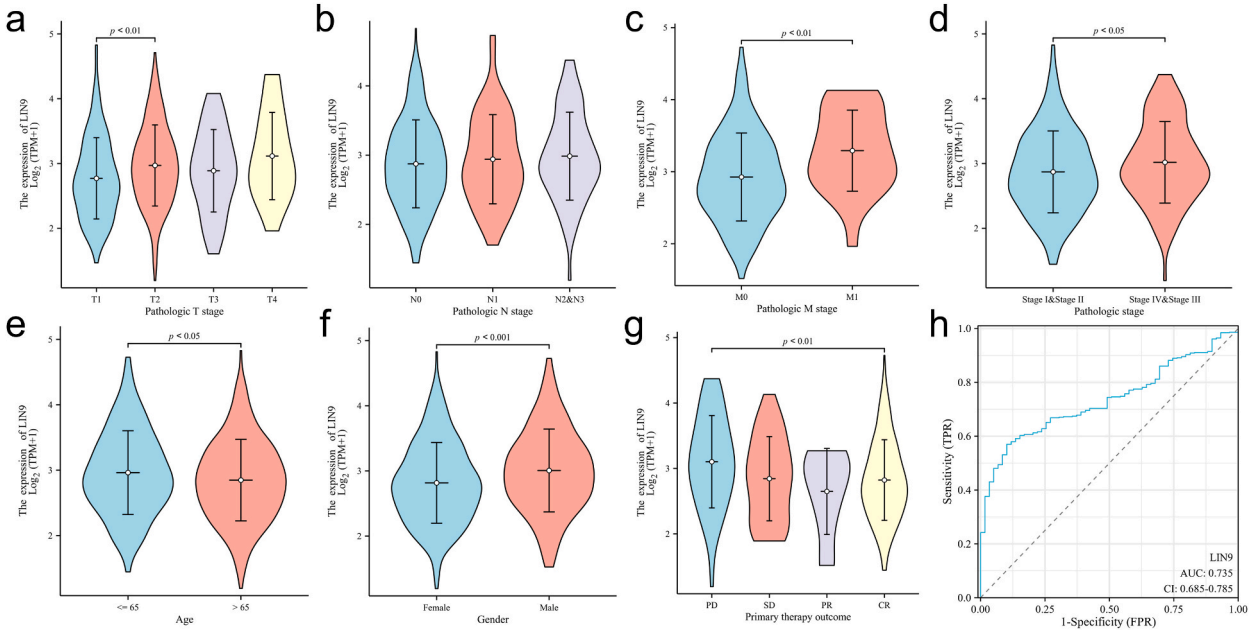

Fig. 4. Relationship between LIN9 expression and clinicopathological features in LUAD. (a) T stage, (b) N stage, (c) M stage, (d) pathological stage, (e) age, (f) gender, (g) primary therapy outcome, (h) and diagnostic ROC curve.

elevated *LIN9* expression is associated with several adverse clinical features, including female gender, distant tumor metastasis, reduced survival time, and poor overall prognosis. To further elucidate the functional role of *LIN9* in LUAD, we performed GO and KEGG pathway analyses using the TCGA dataset. These analyses revealed that *LIN9* is implicated in various biological processes and pathways, including cilium movement, axoneme structure, histone deacetylase binding, and neuroactive ligand-receptor interactions. Histone deacetylase binding is a critical process involving the interaction between histone deacetylases and other proteins. This interaction represents a common mechanism of chromatin modification, which affects chromatin relaxation by removing acetyl groups

Table 3
Univariate regression and multivariate survival methods (OS) of prognostic covariates in patients with LUAD.

Characteristics	Total(N)	Univariate analysis		Multivariate analysis	
		Hazard ratio (95 % CI)	P value	Hazard ratio (95 % CI)	P value
Gender	530				
Female	283	Reference			
Male	247	1.087 (0.816–1.448)	0.569		
Age	520				
≤ 65	257	Reference			
>65	263	1.216 (0.910–1.625)	0.186		
Pathologic stage	522				
Stage I	292	Reference		Reference	
Stage II	123	2.341 (1.638–3.346)	< **0.001**	2.356 (1.648–3.367)	< **0.001**
Stage III	81	3.576 (2.459–5.200)	< **0.001**	3.819 (2.619–5.569)	< **0.001**
Stage IV	26	3.819 (2.211–6.599)	< **0.001**	3.226 (1.852–5.618)	< **0.001**
LIN9	530				
Low	262	Reference		Reference	
High	268	1.570 (1.173–2.100)	**0.002**	1.602 (1.186–2.164)	**0.002**

Table 4
Univariate regression and multivariate survival methods (DSS) of prognostic covariates in patients with LUAD.

Characteristics	Total(N)	Univariate analysis		Multivariate analysis	
		Hazard ratio (95 % CI)	P value	Hazard ratio (95 % CI)	P value
Gender	495				
Female	265	Reference			
Male	230	1.006 (0.699–1.448)	0.975		
Age	485				
≤ 65	245	Reference			
>65	240	1.007 (0.697–1.454)	0.971		
Pathologic stage	487				
Stage I	279	Reference		Reference	
Stage II	114	2.910 (1.863–4.545)	< **0.001**	2.885 (1.847–4.506)	< **0.001**
Stage III	72	3.360 (2.049–5.512)	< **0.001**	3.666 (2.227–6.037)	< **0.001**
Stage IV	22	4.674 (2.393–9.132)	< **0.001**	3.781 (1.914–7.470)	< **0.001**
LIN9	495				
Low	243	Reference		Reference	
High	252	1.815 (1.247–2.641)	**0.002**	1.781 (1.207–2.629)	**0.004**

Table 5
Univariate regression and multivariate survival methods (PFI) of prognostic covariates in patients with LUAD.

Characteristics	Total(N)	Univariate analysis		Multivariate analysis	
		Hazard ratio (95 % CI)	P value	Hazard ratio (95 % CI)	P value
Gender	530				
Female	283	Reference			
Male	247	1.189 (0.914–1.547)	0.197		
Age	520				
≤ 65	257	Reference			
>65	263	1.019 (0.781–1.330)	0.889		
Pathologic stage	522				
Stage I	292	Reference		Reference	
Stage II	123	1.953 (1.434–2.659)	< **0.001**	1.924 (1.412–2.621)	< **0.001**
Stage III	81	1.852 (1.271–2.700)	**0.001**	1.906 (1.307–2.780)	< **0.001**
Stage IV	26	2.103 (1.199–3.687)	**0.009**	1.866 (1.057–3.295)	**0.031**
LIN9	530				
Low	262	Reference		Reference	
High	268	1.432 (1.099–1.866)	**0.008**	1.410 (1.076–1.849)	**0.013**

from histones, thereby influencing gene expression. The interplay between histone deacetylases and acetylation modifications is essential for regulating gene transcription and plays a pivotal role in cellular function and development [21]. Overexpression and recruitment of histone deacetylases play crucial roles in various diseases, particularly tumors [22], indicating that *LIN9* is involved in cancer progression. Moreover, our study demonstrated that *LIN9* is highly expressed in H1395 LUAD cell lines, where it significantly promotes cellular proliferation, migration, and invasion. These data indicate that *LIN9* has a role in both the development of

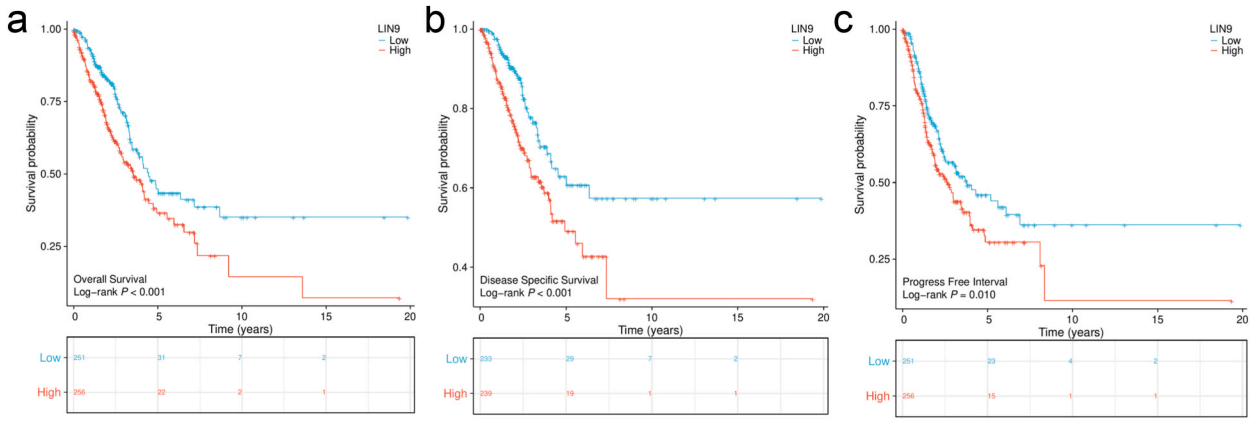

Fig. 5. Relationship between LIN9 expression and prognosis. (a) OS (b) PFI (c) DSS.

malignancy in LUAD and the promotion of its aggressive behavior. This emphasizes the potential of targeting *LIN9* as a therapeutic strategy.

LIN9 dysregulation is implicated in the development of various cancers. Lai et al. [23] reported a significant association between *LIN9* expression levels and resistance to taxane-based treatments in breast cancer. Their findings suggest that variations in *LIN9* expression may influence the effectiveness of taxane therapies, emphasizing its potential function in facilitating medication resistance in breast cancer patients. Notably, the loss of the inhibitory subunit p130 of the DREAM complex was found to accelerate lung tumor formation, whereas depletion of the core subunit LIN9 of the MuvB complex suppressed lung tumor development [24]. Moreover, the target genes of the DREAM complex, *FOXM1* and *ECT2*, have been identified as adverse prognostic biomarkers in patients with lung cancer [25–27]. Therefore, *LIN9* likely plays a pivotal role in this process.

Jasmina et al. [28] demonstrated that *LIN9* plays a crucial role in regulating the expression and proliferation of mitotic genes in embryonic stem cells (ESCs). Their study found that when *LIN9* expression was suppressed, significant changes occurred in the cell cycle distribution of ESCs. Specifically, there was an increase in the number of cells in the G2 and M phases, alongside the appearance of polyploid cells. These alterations collectively led to a deceleration of the ESC cell cycle progression. These results underscore the important role of *LIN9* as a promoter of ESC proliferation, highlighting its essential function in maintaining normal cell cycle dynamics and cell division in these stem cells.

Additionally, the loss of *LIN9* causes a synergistic effect with the large T antigen, which results in the inhibition of anchorage-independent growth and genomic instability. These characteristics are often associated with aggressive malignancies in cancer biology [29]. In our study, *LIN9* expression was notably increased in advanced stages of LUAD. However, the effects of *LIN9* on cancer cells are not unidirectional. *LIN9* exerts tumor-suppressive effects in certain malignancies. In an early study, Gagrica et al. [10] demonstrated that *LIN9* has the potential to inhibit oncogenic transformation, provided that a functional pRB protein is present. This finding suggests a critical dependency of LIN9's tumor-suppressive effects on the integrity of the pRB pathway, underscoring the importance of pRB in modulating LIN9's role in tumorigenesis. The pRB protein, encoded by the retinoblastoma tumor suppressor gene, is essential for regulating various cellular processes, including cell cycle progression, apoptosis, differentiation, and senescence. Its pivotal role in these mechanisms highlights its significance in maintaining cellular homeostasis and preventing uncontrolled cell proliferation, thereby acting as a critical safeguard against tumorigenesis [10,30]. However, it did not participate in pRB-mediated cell cycle arrest.

Our findings diverge from those of previous studies, which suggest that *LIN9* is a tumor suppressor gene in other types of cancers. These contradictory outcomes may stem from the distinct biological functions of *LIN9* in different cellular contexts or various types of cancers. *LIN9* may play varied roles in different tumor microenvironments, which are critical in influencing tumor initiation, progression, and treatment response. These microenvironments encompass a range of factors, including cellular interactions, cell-extracellular matrix interactions, and the availability of nutrients and oxygen. Understanding these diverse functions is essential, as they impact not only the biological behavior of the tumor but also its responsiveness to therapeutic interventions. *LIN9* could potentially regulate different biological pathways in various tumor microenvironments, thereby affecting the biological characteristics of tumors. Furthermore, the performance of *LIN9* across different cancer types might result from its interactions with other factors. In certain cancer types, *LIN9* interacts with factors that promote tumor initiation and progression, thus exerting a tumor-promoting effect. Conversely, in other cancer types, *LIN9* may interact with factors that inhibit tumor development, resulting in a tumor-suppressive role. Additionally, we have to acknowledge that even within the same cancer type, *LIN9* expression and function may differ due to tumor heterogeneity. Tumor heterogeneity encompasses both cellular-level (e.g., the ratio of tumor to non-tumor cells and the proportion of different subtypes of tumor cells) and molecular-level heterogeneities (e.g., differences in gene expression and mutations). These diversities could influence *LIN9* expression and function, resulting in varying roles of *LIN9* in different studies.

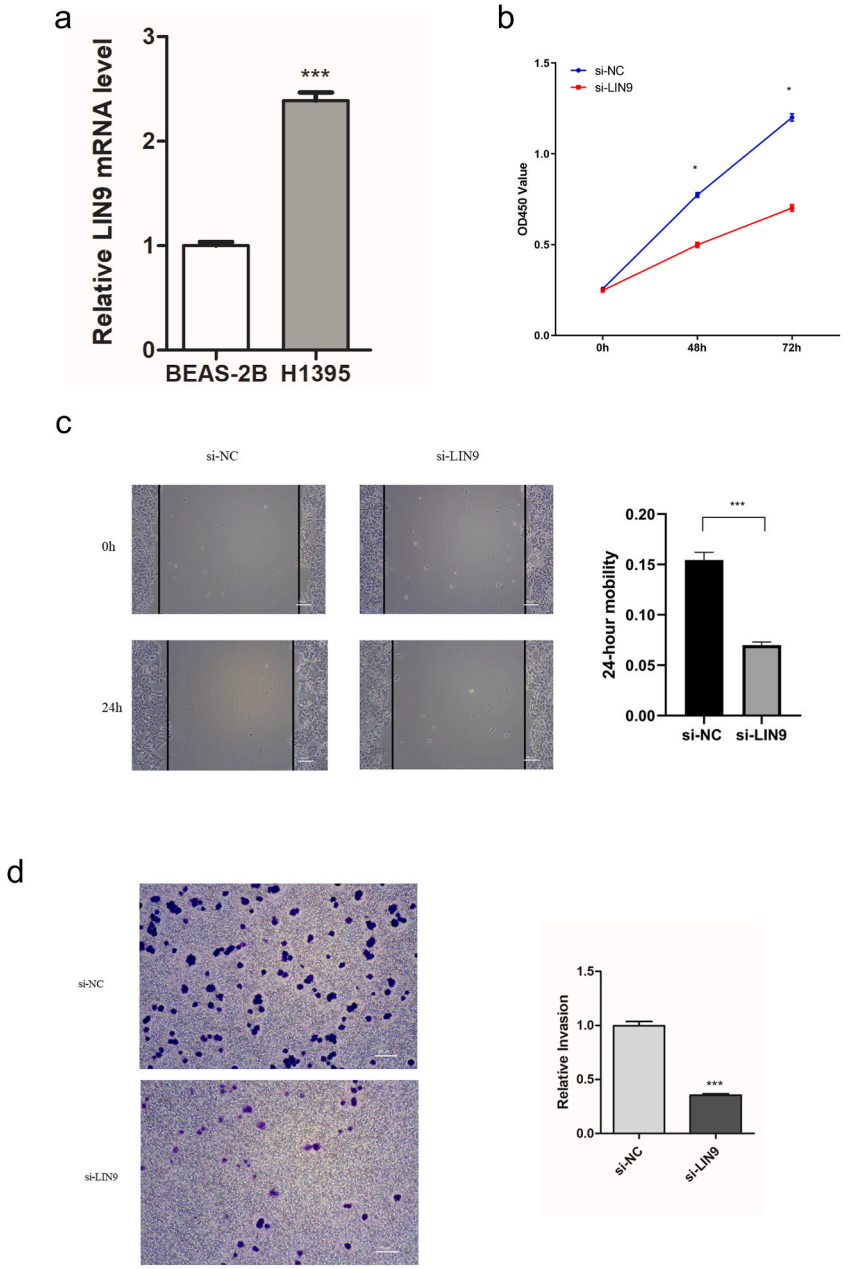

Fig. 6. Cell function assay. (a) Difference in expression of LIN9 between H1395 and BEAS 2B cells. (b) CCK-8 assay. (c) Scratch assay. (d) Transwell assay.

5. Conclusion

The *LIN9* gene has a complex functionality that may significantly contribute to cancer development and treatment strategies. This study identifies *LIN9* as a potential therapeutic target for LUAD. Elevated expression levels of *LIN9* in LUAD could be involved in tumorigenesis through its regulation of the cell cycle and chromatin modifications. High *LIN9* expression might also serve as a predictive marker for clinical prognosis. Increased expression of *LIN9* has been shown to enhance the proliferative, migratory, and invasive capabilities of LUAD cells.

Our study revealed the expression and function of *LIN9* in LUAD; however, our findings diverge from those of previous research. To achieve a more comprehensive understanding, further experiments, detailed analyses, comparisons, and integration with existing studies are imperative. Future research should aim to elucidate the mechanisms and roles of *LIN9* in cancer to offer a crucial theoretical foundation for the development of novel cancer therapeutic strategies.

Ethics approval and consent to participate

Not applicable.

Consent for publication

The co-authors of the study hereby grant their consent for the use of data, photographs, images, and other relevant information pertaining to them for the purpose of publication in the context of this research.

Availability of data and materials

The datasets and materials used or analyzed during the current study are available from the corresponding author upon reasonable request.

Funding

This work was supported by grants from the Science and Technology Innovation Committee of Shenzhen Municipality (Grant No. JCYJ20180228175531145) and the Open Foundation of Shenzhen Huada Institute of Life Sciences (Grant No. BGIRSZ20200003).

CRediT authorship contribution statement

Qinghua Hou: Writing – review & editing, Writing – original draft, Visualization, Validation, Methodology, Investigation, Formal analysis, Data curation. **Yanfeng Zhong:** Validation, Formal analysis, Data curation. **Mengying Liao:** Writing – review & editing, Validation. **Chao Chen:** Writing – review & editing, Writing – original draft, Visualization, Formal analysis. **Yanling Li:** Writing – review & editing, Validation. **Xiaoqing Li:** Writing – review & editing, Validation, Methodology, Formal analysis, Conceptualization. **Jixian Liu:** Writing – review & editing, Visualization, Project administration, Methodology, Funding acquisition, Data curation, Conceptualization.

Declaration of competing interest

The authors declare the following financial interests/personal relationships which may be considered as potential competing interests:Jixian Liu reports financial support was provided by the Science and Technology Innovation Committee of Shenzhen Municipality. If there are other authors, they declare that they have no known competing financial interests or personal relationships that could have appeared to influence the work reported in this paper.

Acknowledgements

We express our heartfelt gratitude to Dr. Liusheng Wu for his valuable recommendation regarding this project.

Appendix A. Supplementary data

Supplementary data to this article can be found online at https://doi.org/10.1016/j.heliyon.2024.e35012.

References

[1] H. Sung, et al., Global cancer statistics 2020: GLOBOCAN estimates of incidence and mortality worldwide for 36 cancers in 185 countries, CA A Cancer J. Clin. 71 (3) (2021) 209–249.
[2] B.D. Hutchinson, et al., Spectrum of lung adenocarcinoma, Semin. Ultrasound CT MR 40 (3) (2019) 255–264.
[3] L. Osmani, et al., Current WHO guidelines and the critical role of immunohistochemical markers in the subclassification of non-small cell lung carcinoma (NSCLC): moving from targeted therapy to immunotherapy, Semin. Cancer Biol. 52 (Pt 1) (2018) 103–109.
[4] P. Xing, et al., Efficacy of crizotinib for advanced ALK-rearranged non-small-cell lung cancer patients with brain metastasis: a multicenter, retrospective study in China, Targeted Oncol. 14 (3) (2019) 325–333.
[5] J.Y. Park, S.H. Jang, Epidemiology of lung cancer in Korea: recent trends, Tuberc. Respir. Dis. 79 (2) (2016) 58–69.
[6] U. Testa, G. Castelli, E. Pelosi, Lung cancers: molecular characterization, clonal heterogeneity and evolution, and cancer stem cells, Cancers 10 (8) (2018).
[7] M. Korenjak, et al., Native E2F/RBF complexes contain Myb-interacting proteins and repress transcription of developmentally controlled E2F target genes, Cell 119 (2) (2004) 181–193.
[8] P.W. Lewis, et al., Identification of a Drosophila Myb-E2F2/RBF transcriptional repressor complex, Genes Dev. 18 (23) (2004) 2929–2940.
[9] A. Blais, et al., Retinoblastoma tumor suppressor protein-dependent methylation of histone H3 lysine 27 is associated with irreversible cell cycle exit, J. Cell Biol. 179 (7) (2007) 1399–1412.
[10] S. Gagrica, et al., Inhibition of oncogenic transformation by mammalian Lin-9, a pRB-associated protein, EMBO J. 23 (23) (2004) 4627–4638.
[11] M.I. Love, W. Huber, S. Anders, Moderated estimation of fold change and dispersion for RNA-seq data with DESeq2, Genome Biol. 15 (12) (2014) 550.
[12] K. Yoshihara, et al., Inferring tumour purity and stromal and immune cell admixture from expression data, Nat. Commun. 4 (2013) 2612.
[13] G. Bindea, et al., Spatiotemporal dynamics of intratumoral immune cells reveal the immune landscape in human cancer, Immunity 39 (4) (2013) 782–795.

[14] K.Z. Guiley, et al., Structural mechanism of Myb-MuvB assembly, Proc. Natl. Acad. Sci. U. S. A. 115 (40) (2018) 10016–10021.
[15] L. Osterloh, et al., The human synMuv-like protein LIN-9 is required for transcription of G2/M genes and for entry into mitosis, EMBO J. 26 (1) (2007) 144–157.
[16] M. Pilkinton, R. Sandoval, O.R. Colamonici, Mammalian Mip/LIN-9 interacts with either the p107, p130/E2F4 repressor complex or B-Myb in a cell cycle-phase-dependent context distinct from the Drosophila dREAM complex, Oncogene 26 (54) (2007) 7535–7543.
[17] F. Schmit, et al., LINC, a human complex that is related to pRB-containing complexes in invertebrates regulates the expression of G2/M genes, Cell Cycle 6 (15) (2007) 1903–1913.
[18] M.A. Kleinschmidt, et al., lin9 is required for mitosis and cell survival during early zebrafish development, J. Biol. Chem. 284 (19) (2009) 13119–13127.
[19] S. Sadasivam, S. Duan, J.A. DeCaprio, The MuvB complex sequentially recruits B-Myb and FoxM1 to promote mitotic gene expression, Genes Dev. 26 (5) (2012) 474–489.
[20] Z. Zhou, et al., Synergy of p53 and Rb deficiency in a conditional mouse model for metastatic prostate cancer, Cancer Res. 66 (16) (2006) 7889–7898.
[21] L. Zhang, et al., Zinc binding groups for histone deacetylase inhibitors, J. Enzym. Inhib. Med. Chem. 33 (1) (2018) 714–721.
[22] P. Marks, et al., Histone deacetylases and cancer: causes and therapies, Nat. Rev. Cancer 1 (3) (2001) 194–202.
[23] H. Lai, et al., LIN9 confers paclitaxel resistance in triple negative breast cancer cells by upregulating CCSAP, Sci. China Life Sci. 63 (3) (2020) 419–428.
[24] B.E. Schaffer, et al., Loss of p130 accelerates tumor development in a mouse model for human small-cell lung carcinoma, Cancer Res. 70 (10) (2010) 3877–3883.
[25] B. Decaesteker, et al., TBX2 is a neuroblastoma core regulatory circuitry component enhancing MYCN/FOXM1 reactivation of DREAM targets, Nat. Commun. 9 (1) (2018) 4866.
[26] S.K. Liang, et al., FOXM1 is required for small cell lung cancer tumorigenesis and associated with poor clinical prognosis, Oncogene 40 (30) (2021) 4847–4858.
[27] X. Bai, et al., Progression and prognostic value of ECT2 in non-small-cell lung cancer and its correlation with PCNA, Cancer Manag. Res. 10 (2018) 4039–4050.
[28] J. Esterlechner, et al., LIN9, a subunit of the DREAM complex, regulates mitotic gene expression and proliferation of embryonic stem cells, PLoS One 8 (5) (2013) e62882.
[29] S. Hauser, et al., Loss of LIN9, a member of the DREAM complex, cooperates with SV40 large T antigen to induce genomic instability and anchorage-independent growth, Oncogene 31 (14) (2012) 1859–1868.
[30] M. Classon, E. Harlow, The retinoblastoma tumour suppressor in development and cancer, Nat. Rev. Cancer 2 (12) (2002) 910–917.